Received: 15 March 2022 | Revised: 26 May 2022 | Accepted: 7 June 2022

DOI: 10.1002/jsp2.1212

RESEARCH ARTICLE

JOR Spine OPEN ACCESS

Axial hypersensitivity is associated with aberrant nerve sprouting in a novel model of disc degeneration in female Sprague Dawley rats

David J. Lillyman | Fei San Lee | Evie C. Barnett | Tyler J. Miller | Moreno Lozano Alvaro | Henry C. Drvol | Rebecca A. Wachs

Department of Biological Systems Engineering, University of Nebraska, Lincoln, Nebraska, USA

Correspondence
Rebecca A. Wachs, 4240 Fair Street, Lincoln, NE, 68583, USA.
Email: rebecca.wachs@unl.edu, https://engineering.unl.edu/bsen/faculty/rebecca-wachs/

Abstract

Chronic low back pain is a global socioeconomic crisis and treatments are lacking in part due to inadequate models. Etiological research suggests that the predominant pathology associated with chronic low back pain is intervertebral disc degeneration. Various research teams have created rat models of disc degeneration, but the clinical translatability of these models has been limited by an absence of robust chronic pain-like behavior. To address this deficit, disc degeneration was induced via an artificial annular tear in female Sprague Dawley rats. The subsequent degeneration, which was allowed to progress for 18-weeks, caused a drastic reduction in disc volume. Furthermore, from week 10 till study conclusion, injured animals exhibited significant axial hypersensitivity. At study end, intervertebral discs were assessed for important characteristics of human degenerated discs: extracellular matrix breakdown, hypocellularity, inflammation, and nerve sprouting. All these aspects were significantly increased in injured animals compared to sham controls. Also of note, 20 significant correlations were detected between selected outcomes including a moderate and highly significant correlation ($R = 0.59$, $p < 0.0004$) between axial hypersensitivity and disc nerve sprouting. These data support this model as a rigorous platform to explore the pathobiology of disc-associated low back pain and to screen treatments.

KEYWORDS

axial hypersensitivity, disc degeneration, disc-associated pain, discogenic pain, grip strength, low back pain, nerve sprouting, open arena, pressure algometry

1 | INTRODUCTION

Low back pain (LBP) is the leading cause of disability worldwide.[1] 84% of people who suffer an episode of LBP will recover, but for 16%, the pain will become chronic and disabling.[2] Chronic LBP increases risk of unemployment, depression, insomnia, suicide, and costs the United States more than $100 billion each year.[3–5] Despite the immense socioeconomic burden of chronic LBP, elucidation of the causal drivers of pain remains incomplete. The most strongly associated factor with chronic LBP is intervertebral disc degeneration.[6] Unfortunately, treatments for disc-associated LBP exhibit poor long-term efficacy.[7–9] The failure of current treatments can be attributed to

a poor understanding of the pathobiology underpinning disc-associated pain and a lack of pre-clinical animal models to screen therapeutics.

In a subset of human patients with LBP, pathological changes in the disc are thought to drive nociception and in turn pain. In these patients, degenerated discs exhibit four important characteristics: (1) extracellular matrix (ECM) breakdown, (2) hypocellularity, (3) aberrant nerve sprouting and (4) inflammation.[10–17] ECM breakdown and hypocellularity result from deleterious nutrient deficiency and altered biomechanics incompatible with tissue homeostasis.[18] LBP disc samples also exhibit high levels of pro-inflammatory mediators and a preponderance of nerves suggesting inflammation and nerve sprouting are involved in LBP genesis.[15,16,19] These four factors provide empirical targets for an animal model of painful disc degeneration.

To be successful, animal models of pain must achieve three criteria: construct validity, face validity, and predictive validity.[20–22] Construct and face validity relate to the replicative accuracy of disease induction and phenotype respectively. Predictive validity describes how well treatment efficacy in a model translates to human efficacy. For a disc-associated LBP model, construct and face validity require pain genesis to relate to pathological shifts in the disc, like nerve sprouting, and for the phenotype to manifest similar to the disability and pain observed in humans. In theory, accurate construct and face validity endow a model with degeneration analogous to the human disease state, making treatments translatable, thereby imparting predictive validity. It is vital that these criteria are achieved in animal models that seek to provide insight for human disease mechanisms and treatments.

Rodents are excellent for pre-clinical models because of their accelerated aging, well-defined behavioral assays, size, and cost.[23] It may be reasoned that pronograde animals like rodents cannot represent the spinal loading of orthograde animals like humans. Interestingly, research suggests the orientation of the spine, whether parallel or perpendicular to gravity, does not largely impact discal pressures.[24–26] This lack of difference is further supported by the similarity of disc rheological properties among rodents, pigs, rabbits, sheep, baboons, and humans.[27–30] For a model aimed at evaluating early stage therapeutics, rats are a stronger candidate than mice because rat discs are around ten times larger and thus are more amenable for injection procedures.[31]

In efforts to create a model of LBP in rats, various research groups have induced disc degeneration with methods such as multilevel injury, cytokine injection, spinal destabilization, and large gauge needle puncture, but the transition from a model of degeneration to a model of chronic LBP has been limited by acute time frames, absence of pain-like behavior, animal sex variability, animal age, and confounding secondary effects.[32–38] Given the state of LBP research, there is a need for a valid rat model of disc-associated pain that is analogous to human disease progression, nociception, pain-like behavior, chronicity, and disc degeneration phenotype.

The objective of this work was to develop a novel rodent model of LBP that comprehensively recapitulates the underpinning pathobiology of disc degeneration and the emergence of pain observed in humans. Due to the similarity between our data and the clinical presentation of disc-associated LBP, this model provides value as a platform for evaluating treatments and exploring the pathobiology of disc-associated LBP.

2 | MATERIALS AND METHODS

2.1 | Animals

36 female, 15-week-old, Sprague Dawley rats were purchased from Envigo and housed with a 12-h light/dark cycle and ad libitum access to food and water. On the day of surgery, the animals were split into three groups of equal size ($n = 12$): sham, 1-scrape, and 6-scrape. After surgery, all animals were weighed and assessed on a weekly basis for overall health. Sample sizes were chosen to ensure sufficient power to detect a 30% decrease in grip strength in injured animals compared to sham animals assuming a standard deviation that was 26% of the mean. At the study conclusion, a total of three animals were excluded from the study (sham: $n = 12$, 1-scrape: $n = 11$, 6-scrape: $n = 10$) due to mis-puncture confirmed by disc volume and H & E data. All animal procedures and assays were in accordance with the National Institute of Health guidelines following PHS Policy on Humane Care and Use of Laboratory Animals and approved by the Institutional Animal Care and Use Committee and the University of Nebraska – Lincoln.

2.2 | Surgical procedure and injury

On the day of surgery, rats were anesthetized, and the lumbar spine was approached ventrally by dissecting through the abdominal cavity and retroperitoneum. The iliac crest was used as a landmark to reliably dissect down to the L5-L6 disc. For sham animals, the L5-L6 was visualized only, and the surgical site was closed in the same manner as injured animals outlined below. For injured animals, the L5-L6 lumbar disc was punctured bilaterally with a strong point dissecting needle (Roboz, RS-6066) with an O.D. of 0.5 mm set to a length of 3 mm. The exact needle length was predetermined based on μCT data to ensure that the needle length did not exceed the diameter of the smallest L5-L6 disc in all animals. While the needle was within the disc, it was swept back and forth along a 90° arc once or six times in the transverse plane for 1-scrape and 6-scrape animals respectively. A simple continuous and subcutaneous suture pattern were used to close the abdominal wall and the skin respectively. Buprenorphine SR (0.75 mg/kg) was administered once post-op for pain and animals were rested for two weeks following surgery to enable healing. All animals displayed mild pica behavior, that is, bedding consumption, after surgery but this behavior resolved within 72 h.

2.3 | Disc volume

The L5-L6 disc volume was quantified using the Quantum GX2 μCT Imaging System and Analyze 13.0 (Analyze Direct). In short, the rat

lumbar spine was radiographed by placing anesthetized animals in the supine position and scanning for 2-min with 90 kV power, 88 μA tube current, 72 mm FOV, 144 um voxel size, and a Cu 0.06 + Al 0.05 x-ray filter. VOX files were then removed from the μCT computer and analyzed in Analyze 13.0. To begin processing, raw VOX files from the μCT scans were processed using a high pass threshold to remove all non-bony signal. After the scans were reduced to only bony tissue using the software filter, the intervertebral disc space was colored in every coronal plane where the adjacent vertebral bodies were present using a manual draw tool. The slices of colored intervertebral disc space between the L5 and L6 vertebral bodies were then concatenated, smoothed using a built-in function and saved as an object map. The volume of the object map of these concatenated colored planes was quantified using a built-in software analysis. This quantification was based on a previously established method developed in our lab (under review).

2.4 | Behavioral tests

For all behavioral tests, animals were acclimated prior to the study commencement to the assay apparatuses and experimenters over the course of three weeks with at least 1 h of acclimation to each assay apparatus prior to any data collection. All assays except grip strength were performed under red light to minimize animal stress. No more than two behavioral assays were performed on a given day. Experimenters were blinded to animal treatment and all animals were assigned to groups by an unblinded observer.

2.5 | Von Frey mechanical hypersensitivity

Hypersensitivity to punctate mechanical stimulation in both hind paws was quantified using an electronic von Frey aesthesiometer (IITC, 2391) with a rigid tip with an outer diameter of 0.8 mm. Briefly, four animals at a time were allowed to acclimate for 15 min in clear acrylic chambers placed on a metal grid (IITC, 410). Withdraw threshold was assessed bilaterally by sequentially applying the probe to the right hind paw of all animals followed by the left hind paw of all animals. This process was performed five times with approximately 5 min of rest between each test for a total of 10 values (5 left, 5 right). The withdraw threshold was calculated by taking the combined left and right average of the final four measurements (eight subsamples for each animal). All withdraw thresholds were log transformed to achieve normality and then normalized to baseline to reduce variability.

2.6 | Grip strength axial hypersensitivity

Hypersensitivity to axial strain was quantified using a grip strength apparatus (Columbus Instruments, 1027SR). All animals were allowed to acclimate to the testing room for 15 min prior to testing. Animals were picked up by grasping the hind quarter and then allowed to grip a metal wire mesh attached to the grip strength force sensor. The experimenter's grip was then transitioned to the base of the tail and the animal was gently pulled backward until it released the metal wire mesh. This process was repeated three times and the average max force (N) was used as the grip strength. All withdraw grip strength thresholds were log transformed to achieve normality and then normalized to baseline to reduce variability.

2.7 | Pressure algometry deep tissue hypersensitivity

Hypersensitivity around the L5-L6 motion segment was measured using an electronic von Frey aesthesiometer (IITC, 2391) with a blunt tip. All animals were allowed to acclimate to the testing room for 15 min prior to testing. Each animal was sequentially hooded inside a clean cotton t-shirt such that the entire animal was covered. The animal was then loosely constrained by one experimenter while another experimenter applied the blunt probe to the dorsal L5-L6 skin and slowly increased the pressure until the animal exhibited a nocifensive response. The L5-L6 skin area was ascertained by palpating along the caudal spinal curvature to locate the area of skin directly superficial to the spinous processes just caudal of the iliac crest. Positive responses included rolling, rapid movement, and vocalization. Two measurements were collected for each animal and the average was used as the deep tissue pressure threshold. All animal thresholds were normalized to baselines to reduce variability.

2.8 | Open field test

Spontaneous pain-like behavior was evaluated using the open field test with custom built acrylic 2' × 2' × 2' black, opaque arenas. All animals were allowed to acclimate to the testing room for 15 min prior to testing. Animals were individually placed in arenas illuminated by overhead red lighting and allowed to explore for 30 min while recorded by an overhead low-light camera (ALPCAM). The middle 20 min of each video was analyzed using Ethovision (Noldus) for total distance traveled, time spent rearing unsupported, time spent rearing supported, time spent grooming, max velocity, average turn angle, and max turn angle. All data were normalized to baselines to reduce variability.

2.9 | Motion segment processing

At the study conclusion, L5-L6 discs were resected, fixed, decalcified, embedded, and sectioned to provide motion segment sections for histological and immunohistochemical processing. In brief, animals were euthanized using CO_2 overdose with cardiac puncture as a secondary measure, and the lumbar spine was resected, and cleaned using bone cutters. The L5-L6 motion segment was isolated from the cleaned

spine using a fine-tooth hand saw. After, motion segments were placed in a 6-well plate with 5 ml of 4% paraformaldehyde (PFA) at room temperature for 24 h with agitation. After fixation, motion segments were washed 3 × 15 min with 1X PBS and decalcified for 18 h in 3 ml of Immunocal (StatLab 1414–32) at room temperature on an orbital shaker plate at 250 RPM. Decalcified segments were then washed 3 × 15 min with 1X PBS and cryoprotected using an overnight 30% sucrose soak. Finally, sections were embedded in Optimal Cutting Temperature Compound (Tissue-Tek) and sectioned in the sagittal plane at 15 and 40 μm thicknesses.

2.10 | Histological processing

15 μm sections from L5-L6 motion segments were processed using H&E according to standard protocols. In short, sections were post fixed for 15 min with 4% PFA, washed with 1X PBS, and stained with hematoxylin. Following hematoxylin staining, sections were washed with 1X PBS, differentiated using acid alcohol, blued with a sodium acetate solution, dehydrated using an alcohol gradient, counterstained with eosin, dehydrated with xylenes, and mounted using Permount (Fisher Scientific SP15-100). Three motion segment sections from each animal were stained using the aforementioned process and each motion segment was imaged by collecting and stitching two images taken with a 10X objective on a Zeiss Axio Observer A1 Inverted Microscope (Carl Zeiss Microscopy, Inc.).

2.11 | Immunohistochemistry

15 μm and 40 μm sections from L5-L6 motion segments were processed using IHC to visualize inflammatory cytokines and nerve fibers respectively. Both assessments employed the same IHC protocol but used different primary and secondary antibodies. Sections were post-fixed with 4% PFA for 15 min, washed 2 × 5 min with 1X PBS, 2 × 5 min with PBST (1X PBS + 0.01% Tween-20), blocked for 1 hwith blocking buffer (1X PBS + 3% goat serum +0.3% Triton X-100), and incubated in blocking buffer with either 1:100 mouse-derived anti-rat TNF-α (Santa Cruz SC-52746) or 1:500 mouse-derived anti-rat NF-H (Abcam ab528399), 1:100 rabbit-derived anti-rat PGP9.5 (Abcam Ab108896), and 1:1000 chicken-derived anti-rat peripherin (Novus NBP1-05423) for 16 h. After primary incubation, sections were washed 3 × 15 min with PBST and incubated in blocking buffer for 1 hwith 1:500 goat-derived anti-mouse AF488 (Abcam Ab150177) and, in the case of nerve IHC, anti-rabbit AF555 (Abcam B150086) and anti-chicken AF647 (ThermoFisher A21449). Following secondary incubation, sections were washed 3 × 15 min in PBST and incubated with DAPI (ThermoFisher D1306) 1:1000 in PBS for 15 min followed by a 3 × 5-min wash in 1X PBS and then mounted using Prolong Gold (ThermoFisher P36930). Three motion segment sections from each L5-L6 disc were processed using the aforementioned method and the entire motion segment images were created by stitching six tiles collected on a Cytation 5 (BioTek) at 4X magnification in the following channels or emission/excitations: brightfield, 377/447 (DAPI), 445/510 (AF488), 531/593 (AF555), and 628/685 (AF647).

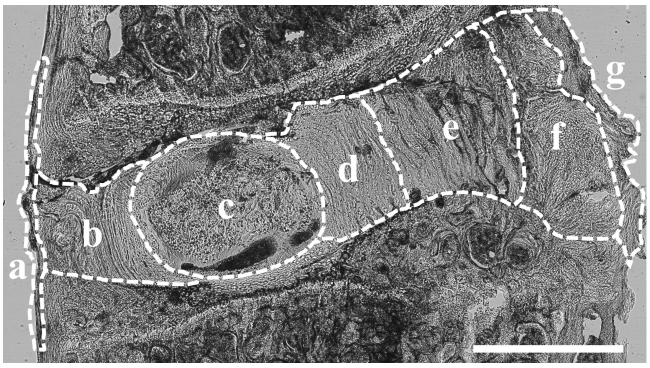

FIGURE 1 Disc breakout by regions. Region specific quantification for IHC analysis was accomplished by breaking the disc into seven regions. These regions are overlaid on the brightfield image: a = dorsal ligament, b = dorsal AF, c = NP, d = ventral AF inner 2/3, e = ventral AF outer 1/3, f = granulation, g = ventral ligament. Scale bar = 1 mm

2.12 | Image analysis

H&E, nerve fiber IHC, inflammatory cytokine IHC, and cellularity outcomes were evaluated on three sections from each animal for a total of ~99 images for each process. Three blinded observers were employed for H&E and nerve fiber scoring. H&E sections were graded according to a rubric delineated by Lai et al. 2021 excepting NP cell morphology.[39] To accomplish this process, disc morphology was broken into NP shape, NP area, NP cell number, NP cell morphology, NP-AF border appearance, AF lamellar organization, AF tears/fissure/disruptions and endplate disruptions/microfractures/ossification. Each of these subcriteria was evaluated on a 0–2 basis, with 0 implying a healthy tissue and 2 implying a degenerated tissue. Observers were trained on example H&E images until the interobserver agreement exceeded 75%. For nerve fiber and inflammatory cytokine IHC, the disc was split into seven zones: dorsal ligament, dorsal AF, NP, ventral AF inner two thirds, ventral AF outer one third, granulation, and ventral ligament (Figure 1). These zones are outlined in Figure 1. For nerve fiber IHC, each zone was scored a 0, 1, or 2 based on the presence of 0, 1–3, and 4+ nerve fibers respectively. For nerve IHC scoring, nerve fibers within the ligamentous tissue served as ground truths for immunopositivity. A fiber was recognized as either a cross-section, represented by a circular area of intense immunopositivity, or a longitudinal section, defined by a tract of immunopositivity. Furthermore, for nerve IHC grading, graders were asked to verify immunopositivity observed in PGP9.5 by comparing to NF-H and peripherin immunopositivity. All images were individually scored on a high dynamic range IPS display by three blinded evaluators and each final animal score was calculated by taking an average of all three motion segments across the three

TABLE 1 Overview of the data included in the Pearson correlation and principal component analysis (PCA)

Outcome	Disc volume	Grip strength	Von frey	Pressure algometry	Distance traveled	Summed H&E	Disc nerve	Ligament cellularity	Disc cellularity	Disc TNF-α
Date	Week 18	Week 18	Week 18	Week 18	Week 18	Sum of all individual H&E scores	Sum of NP and AF scores	Ligament cellularity only scores	Average of NP and AF cellularity	Average of AF TNF-α + cells

observers. Cell counting for cellularity and inflammatory cytokine IHC analyses were processed by a single blinded observer using ImageJ. DAPI images were processed in ImageJ according to standard methods to approximate number of cells.[40] For inflammatory cytokine IHC, total number of cells and area of each zone was quantified using ImageJ using the same method as DAPI counting with two exceptions. For inflammation quantification, the particle maximum area set to 200 μm^2 and the intensity threshold for 8-bit image conversion was set to 50-infinity.

2.13 | Correlation and principal component analysis

The Pearson correlation analysis and principal component analysis (PCA) were performed in GraphPad Prism 9. For both analyses, week 18 μCT and behavioral data were used. The data used from the H&E, disc nerve, and disc cellularity were the disc only values, that is, the combination of the AF and NP values (Figure 5E, 6E, 7E). The disc inflammation data were composed only of the average number of TNF-α positive cells in the AF (Figure 8E). The ligament cellularity was composed of the ventral and dorsal ligament cell number average. A visual overview of the data used can be seen in Table 1. For the grip strength versus nerve score analysis, week 16 and week 18 grip strength data were averaged to get a better approximation of the mean and these data were correlated to the disc (NP + AF) nerve score. All animals from all treatments were included in both the correlation and PCA data. The data across the three treatments represented a spectrum of degeneration and thus associative analyses like the Pearson correlation and PCA were particularly useful in identifying what consequences of disc injury related to one another at the 18-week time point.

2.14 | Statistical analysis

All data are presented as mean ± standard deviation. Data were analyzed using GraphPad Prism 9. Normality was assessed using a Shapiro–Wilk test. Behavioral and disc volume data were analyzed using a two-way ANOVA with Dunnett's post hoc. Each region in cellularity and inflammation data was analyzed using a one-way ANOVA with a Dunnett's post hoc. H&E and nerve IHC was analyzed using a Kruskal–Wallis test with a Dunn's post hoc. Results were considered statistically different when $p < 0.05$.

3 | RESULTS

3.1 | Model overview

Sprague–Dawley rats were selected because of their outbred genetics, and well-characterized assays for pain-like behavior assessment.[41] To date, the overwhelming majority of rodent models of disc degeneration and LBP have been created in male animals.[41,42] In contrast, female animals were chosen for this study because LBP is 30% more prevalent in aged women than men.[43] Animals were injured at 18-weeks of age to ensure all animals had reached osseous maturity such that growth related bony remodeling would not confound the model.[44] In humans, disc degeneration rarely occurs prior to osseous maturity emphasizing the importance of a correct skeletal growth state. This study entailed 3 weeks of acclimation and baseline data collection, surgery, and 18 weeks of observation (Figure 2A). During surgery, the L5-L6 disc was visualized in all animals via a ventral approach after dissecting through the abdominal wall and retroperitoneum (Figure 2B). The L5-L6 disc was the target for injury because it is analogous to the L4-L5 disc in humans which is the most common level of disc degeneration.[45] For injured animals, a hard point microdissecting needle was used to bilaterally puncture and disrupt the macrostructure of the disc (Figure 2C). The needle was rotated along a 90-degree arc in the transverse plane once for animals in the 1-scrape injury and six times for animals in the 6-scrape injury. This injury resulted in bilateral, complete annular fissures along with internal macrostructure disruption from the scraping motion. Annular fissures have been described as major contributors and predictors of progressive lumbar disc degeneration and LBP in humans.[46]

3.2 | Injury results in disc volume loss

To evaluate disc degeneration in real time, microcomputed tomography (μCT) was used to calculate the L5-L6 disc volume at 0, 2, 4, 8, 12, and 18 weeks. This method entailed masking the intervertebral disc space between the L5 and L6 vertebral bodies to create a 3D reconstruction of the disc for which the volume was calculated (Figure 3A,B). Disc volume in both 1-scrape and 6-scrape groups drastically dropped after surgery and remained significantly decreased compared to sham at all measured time points up to week 18 (Figure 3C). The disc volume method detected highly significant differences between sham and injured animals at weeks 2, 4, 8, and 12 ($p < 0.0001$–0.0097). These data confirmed that the 1-scrape and

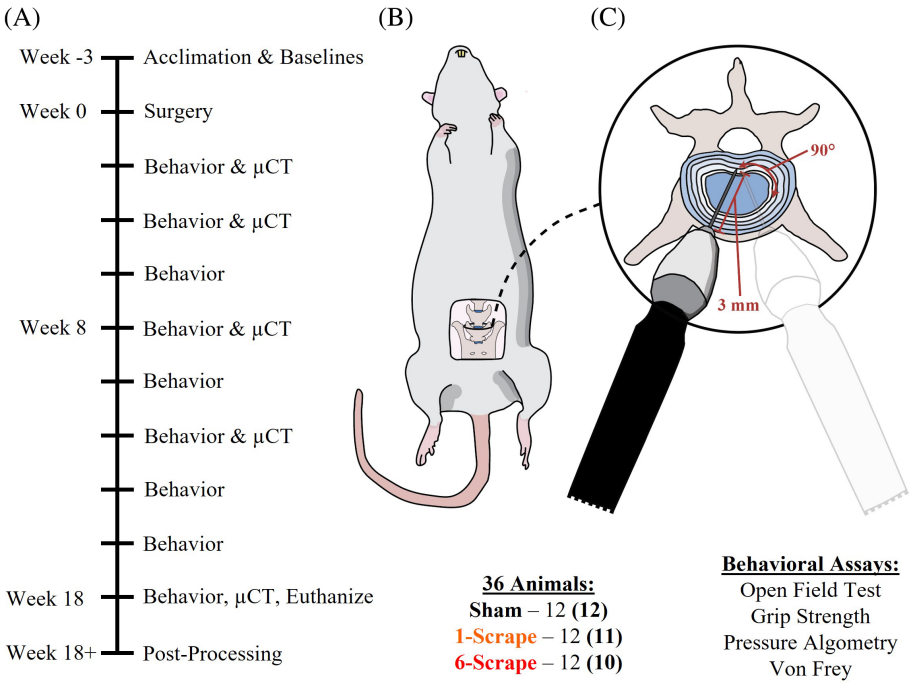

FIGURE 2 Animal study overview. (A) Timeline of the study. Animals were acclimated for 3 weeks before collecting baselines. Behavior testing was done every other week and µCT was performed on weeks 0, 2, 4, 8, 12, and 18. (B) Graphic of the surgical process. The L5-L6 intervertebral disc was approached ventrally through the abdomen. (C) Graphic of the important aspects of the injury process. The needle was inserted to a depth of 3 mm and swept back and forth in the transverse plane along a 90° arc – this process was performed bilaterally. The transparent needle represents the contralateral location of needle insertion. One animal from the 1-scrape and two animals from the 6-scrape group were excluded from the study due to mis-puncture. Final animal number per group is shown in bold in parenthesis

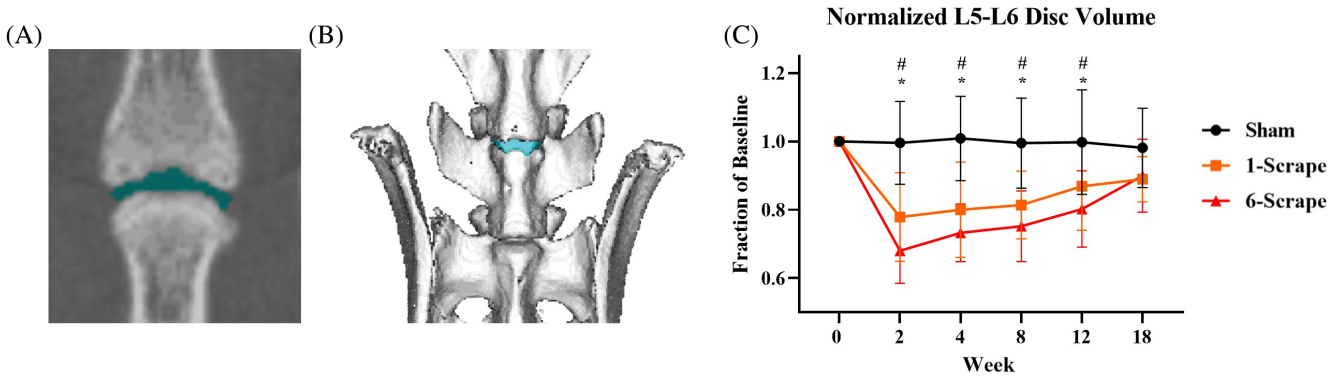

FIGURE 3 Disc volume significantly decreases after injury. (A) 2D rendering with the L5-L6 intervertebral disc space colored in blue. Approximately 20 of these colored slices were concatenated to make the final object map for which the volume was determined. (B) 3D rendering of the rat lumbosacral spine with the L5-L6 disc object map colored in blue. (C) Normalized L5-L6 disc volume of all animal groups. Both injured groups displayed significantly decreased disc volumes compared to sham through week 12. Significant differences were not observed in week 18 due to the gradual increase of disc volume in injured animals occurring after week 2. Data are shown as mean with standard deviation ($n = 10–12$ per group). # = $p < 0.05$ sham versus 1-scrape. * = $p < 0.05$ sham versus 6-scrape

6-scrape injury compromised the hydrostatic equilibrium the disc, resulting in persistent decreased disc volume.

3.3 | Injury produces hypersensitivity in evoked pain-like behavior

A battery of pain-like behavior assessments was performed on a biweekly basis to assess the impact of disc injury on animal function. Grip strength, pressure algometry, and von Frey assays measured evoked pain-like behavior, entailing direct manipulation of the animal by an experimenter whereas the open field test measured spontaneous pain-like behavior, involving only observation.

The grip strength assay specifically assessed grip strength impairment mediated by axial strain hypersensitivity (Figure 4A).[47] Of note, axial hypersensitivity is commonly observed in patients suffering disc-associated LBP and has been observed in mouse models of spontaneous and induced disc degeneration.[48–51] 1-scrape animals exhibited significantly greater hypersensitivity compared to sham only in weeks 12 and 16 whereas 6-scrape animals exhibited increased hypersensitivity in week 6 and at all time points from week 10 to 18 (Figure 4B). The differences observed in grip strength demonstrated axial strain in injured animals resulted in increased axial pain-like behavior.

Hypersensitivity to deep pressure was determined using a modified pressure algometry assay (Figure 4C).[52] This assay was employed because deep pressure hypersensitivity has been previously described

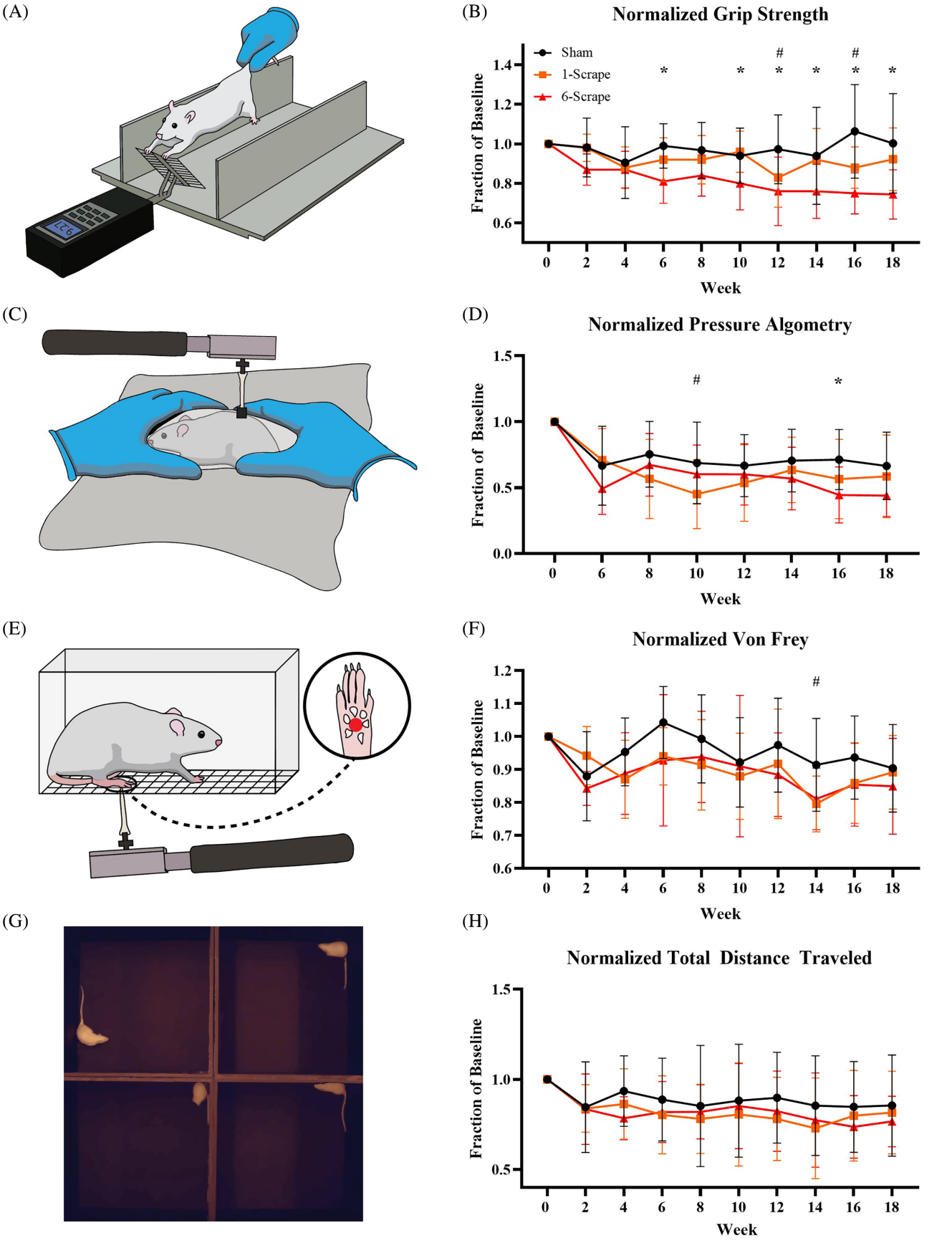

FIGURE 4 Legend on next page.

as highly determinative of LBP in humans and has been used in another model of painful disc degeneration.[37,53] Weeks 2 and 4 data were not included because animals displayed strong aversive responses to the assay in these weeks. Injured animals exhibited significantly increased hypersensitivity compared to sham animals only at week 10 for 1-scrape and in week 16 (week 18 $p < 0.052$) for 6-scrape animals (Figure 4D). This assay was successful in detecting differences between the sham and injured animals but the failure of sham to return to baseline indicated the measurement was influenced by both surgery and injury.

The von Frey assay was performed to measure referred hypersensitivity and to rule out radiculopathy confounds (Figure 4E). Radiculopathy development was a concern because the needle used to injure the disc could have errantly damaged spinal roots. Fortunately, unilateral differences in withdraw threshold were not observed indicating that the model was not confounded by spinal root lesions. Referred hypersensitivity in the hind paw was anticipated in this model because L5 DRG neurons innervate the hind paw footpad and the dorsal and dorsolateral outer AF, implicating cross-sensitization as a contributor to pain-like behavior.[54–58] Sham animals consistently had higher withdraw thresholds than injured animals, but these differences failed to reach significance at all time points except for week 14 between sham and 1-scrape. These data indicated that referred hypersensitivity in the hind-paw did not develop after disc injury, complementing and contrasting prior models in female and male rats respectively.[59,60]

The open field test was performed to evaluate the changes in spontaneous pain-like behavior (Figure 4G). LBP increases movement disability in humans so it was presumed that animals suffering disc-associated pain may exhibit similar changes.[61] No significant differences were observed at any time point in all quantifications including total distance traveled, time spent rearing unsupported, time spent rearing supported, time spent grooming, max velocity, average turn angle, and max turn angle (Figure 4H and data not shown). During analysis, it was determined that a slight difference in box illumination due to the arenas not being symmetrically arranged under the overhead lighting affected the roaming behavior (Figure 4G). The data collected from this assay could be improved in the future by addressing this confound.

These pain-like behavior data indicate that the 1-scrape and 6-scrape injury resulted in hypersensitivity to axial strain and pressure but did not result in detectable changes in referred hypersensitivity, radiculopathy, nor changes in spontaneous open field behavior. All non-normalized data can be found in Figure S1.

3.4 | Injury results in disc degeneration and ECM breakdown

At the study conclusion, all animals were euthanized, and motion segment sections were stained with hematoxylin and eosin (H&E) to grade morphological signs of disc degeneration according to a previously established method.[39] NP cell morphology was omitted from the criteria outline by Lai et al. because section thickness (15 μm) made grading this feature unfeasible. Sham animal discs contained healthy, GAG rich NPs and AFs with regularly spaced, uniform lamellae (Figure 5A). All animals displayed signs of end plate ossification highlighted by the arrowhead in box II, presumably due to natural aging (Figure 5A-II). Both 1-scrape and 6-scrape animals exhibited less hematoxylin staining in the NP compared to sham, indicating a loss of glycosaminoglycans and cell nuclei (Figure 5B,C). Hypertrophic cells identified by enlarged nuclei were visible in the AF of injured animals close to hypocellular tissue around the needle tract (Figure 5B-III arrowhead and Figure S4). All degenerated discs contained granulation tissue between the ventral margin of the disc and ventral ligament (Figure 5B,C-V arrowhead). Interestingly, multiple animal motion segments across both injury groups contained ongoing herniations, one of which can be seen in box IV (Figure 5B-IV arrowhead). To score each section, NP shape, NP area, NP cell number, NP border appearance, AF lamellar organization, AF tears/fissure/disruptions, and endplate ossification were graded on a 3-point scale. Individual criteria for H&E scores measured significantly increased degeneration in all criteria between injured and sham animals except the end plate (Figure 5D). The summation of all individual scores also confirmed significantly increased overall degeneration in injured animals (Figure 5E). In summary, the H&E data demonstrated the 1-scrape and 6-scrape injury induced disc degeneration as measured by an established semi-quantitative protocol.

3.5 | Injury results in disc hypocellularity

Another important aspect of human disc degeneration is disc hypocellularity.[62] As a proxy for cells, nuclei were counted using an automated analysis of DAPI staining. The NP areas in sham animal sections were densely packed with cells and the AF displayed bands of cells consistent with the lamellar structure (Figure 6A). Conversely, injured animal sections exhibited sparce cellularity in the AF, particularly around the site of needle insertion (Figure 6B-IV,C-VI). The NP of

FIGURE 4 Disc injury results in evoked pain-like behavior hypersensitivity. Evoked pain-like behavior assays: grip strength (A and B), pressure algometry (C and D) von Frey (E and F). (B) Normalized grip strength data. 6-scrape animals developed significant hypersensitivity compared to sham animals that persisted for 8 weeks. 1-scrape animals displayed hypersensitivity compared to sham in weeks 12 and 16. (D) Normalized pressure algometry data. 6-scrape animals exhibited significant deep pressure hypersensitivity compared to sham animals in weeks 16 but not week 18 ($p < 0.052$). 1-scrape animals exhibited significant hypersensitivity in week 10 compared to sham. (F) Normalized combined left and right hind-paw von Frey data. The average injured animal thresholds were consistently lower than sham animals but failed to reach significance except in week 14 compared to 1-scrape. (G) Screen capture of animal spontaneous pain-like behavior measured in the open field test. (H) Total distance traveled by the animals in the open field. No significant differences were observed. Data are shown as mean with standard deviation ($n = 10–12$ per group). # = $p < 0.05$ sham versus 1-scrape. * = $p < 0.05$ sham versus 6-scrape

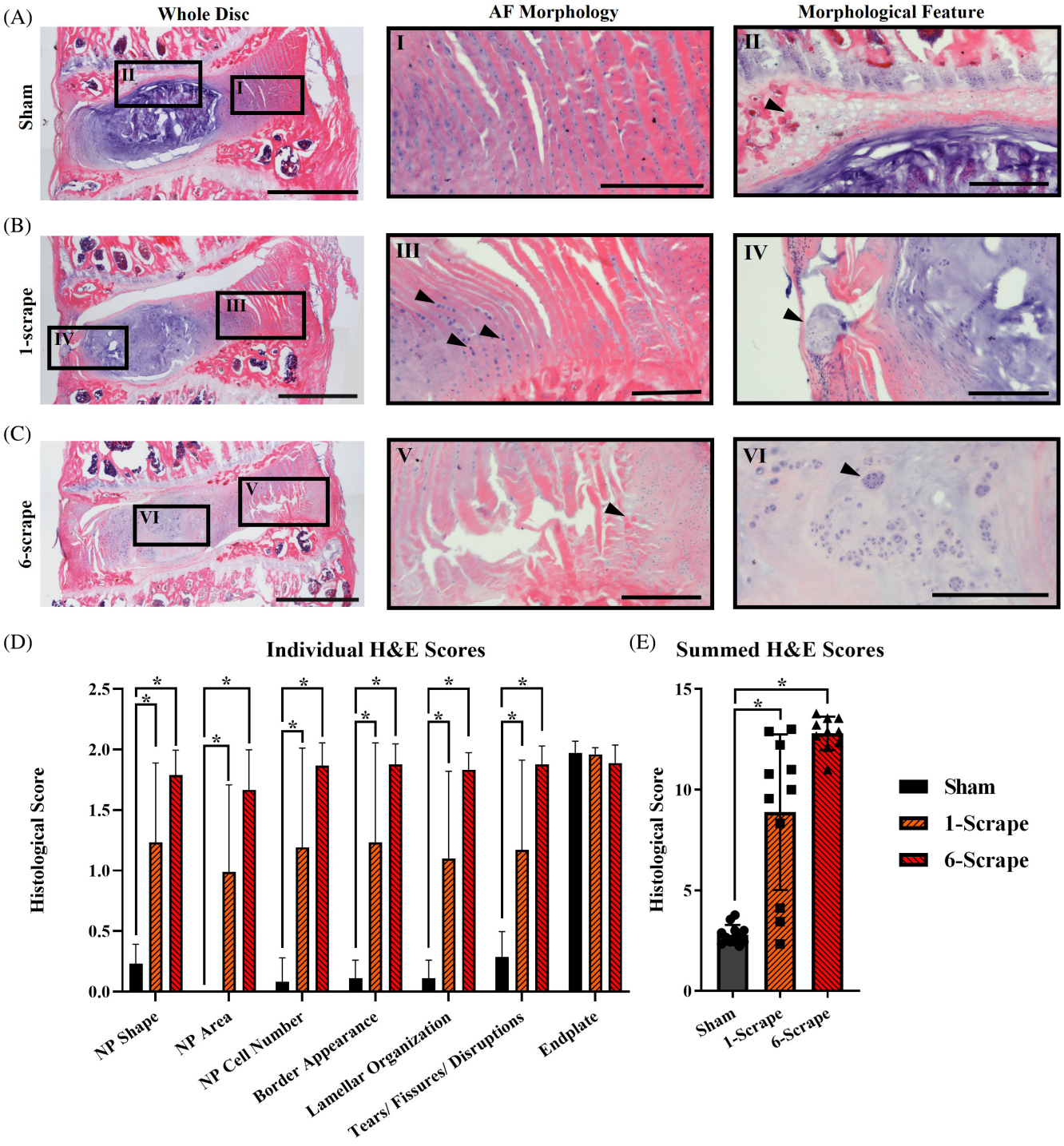

FIGURE 5 Injury to the disc results in disc degeneration. Representative H&E images from the sham group (A), 1-scrape group (B), and 6-scrape group (C). (A) ROI box I draws focus to appearance of a healthy AF structure present in sham animals. All animals exhibited endplate degeneration as highlighted by the arrowhead in ROI box II. (B) ROI box III focuses on the hypocellularity and disruption of the AF in 1-scrape animals. Arrowhead points to hypertrophic cells in the AF. ROI box IV highlights cellular infiltrate present around an ongoing NP herniation. Evidence of these herniations were found in injured discs across both 1-scrape and 6-scrape animals (C) The ROI box V arrowhead points to granulation tissue present on the ventral margin, between the AF and ventral ligament in 6-scrape animals. ROI box VI shows the hypocellularity of degenerated NP tissue and the arrowhead points to a group of NP cells sequestered in a lacuna. Disc image scale bar = 1 mm. ROI box scale bar = 250 μm. (D) Summary of the H&E scores broken down by individual criteria. 1-scrape and 6-scrape scores were significantly higher compared to sham in all categories except end plate. 6-scrape injury resulted in 50% higher average H&E scores compared to 1-scrape, but this failed to reach significance ($p < 0.09$) (E) Summed averages of the individual H&E scores. 1-scrape and 6-scrape scores were significantly higher than sham. The bimodal distribution of scores in the 1-scrape animal group was accounted for by partial healing of the injury defect in three of the 1-scrape animals. Data are shown as mean with standard deviation ($n = 10–12$ per group). * = $p < 0.05$ sham versus 6-scrape

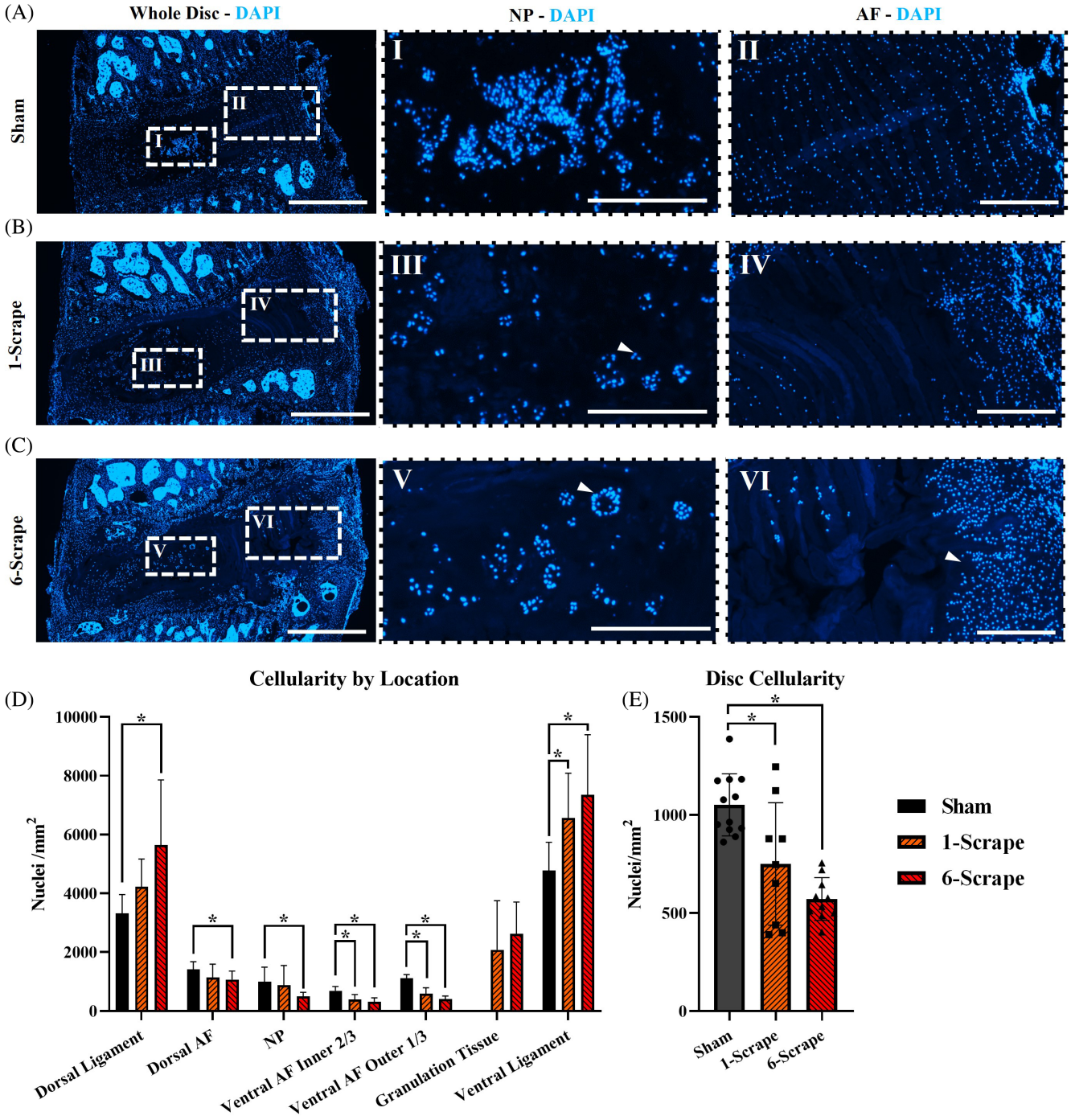

FIGURE 6 Degenerated discs are hypocellular. Representative cellularity (DAPI) images from the sham group (A), 1-scrape group (B), and 6-scrape group (C). (A) Sham animals exhibited dense cellularity in the NP and AF as shown in ROI boxes I and II. (B) 1-scrape animals displayed NP hypocellularity with cells predominantly isolated to lacunae (arrowhead), box III. Box IV highlights the AF hypocellularity. (C) 6-scrape animals exhibited widespread hypocellularity. Box V focuses on the loss of cells in the NP and highlights the isolation of remaining cells to lacunae (arrowheads) like box III in 1-scrape animals. Finally, box VI emphasizes the hypocellularity of the AF around the needle tract and the presence of thick granulation tissue (arrowhead) between the ligament and ventral AF. Whole disc image scale bar = 1 mm. ROI box scale bar = 250 μm. (D) Summary of the cellularity scores broken down by zones. 6-scrape ligamentous tissue was hypercellular compared to sham. All disc zones in 6-scrape animals were hypocellular compared to sham. 1-scrape sections exhibited hypocellularity in the ventral AF and hypercellularity in the ventral ligament. (E) Average of the NP and AF cellularity averages. Disc tissue from 1-scrape and 6-scrape animals was significantly more hypocellular than sham tissue. Data are shown as mean with standard deviation. Two animals from the 1-scrape were excluded due to a lack of usable sections ($n = 9–12$ per group). Significant differences between groups were assessed using a one-way ANOVA. # = $p < 0.05$ sham versus 1-scrape. * = $p < 0.05$ sham versus 6-scrape

6-scrape and 1-scrape sections contained nuclei sequestered to lacunae as noted by the arrowheads in boxes III and V (Figure 6B, C). Granulation tissue, dense with cells, was present in almost all injured animals and can be seen at the arrowhead in box VI (Figure 6C). To quantitatively assess differences, nuclei number was counted using the same region scheme as the nerve IHC analysis. Compared to sham animals, 1-scrape disc tissue was significantly less cellular in the ventral AF but was more cellular in the ventral ligament (Figure 6D). 6-scrape animals displayed significantly higher cellularity in both ligaments but significantly lower cellularity in all regions of the disc compared to sham animals (Figure 6D). The average cellular density of the ventral AF, NP, and dorsal AF was also computed, and both injured groups exhibited significantly lower cell density compared to sham (Figure 6E). This cellularity analysis confirmed that the 1-scrape and 6-scrape injury created a disc environment incompatible with cell survival, like that observed in humans.

3.6 | Injury increases nerve sprouting into the disc

To assess if aberrant nerve sprouting coincided with disc degeneration, like in humans, motion segment sections were processed using immunohistochemistry (IHC) to visualize PGP9.5 (pan neuronal marker), the heavy chain of neurofilament (NF-H), and peripherin (small diameter fiber marker). NF-H and peripherin were included to differentiate nerve fibers, but after processing and validation in DRG sections, it was discovered that unphosphorylated NF-H is expressed across most fiber types in rats limiting its ability to differentiate fibers, and this phenomenon was further suggested by neurobiology research.[63–66] Expectedly, all animals exhibited consistent immunopositivity in the dorsal and ventral ligaments as these structures require innervation for proprioception.[67] Sham animal sections displayed little immunopositivity for any neuronal marker within the disc, but when present, nerves were predominantly in the outer layers of the dorsal AF as noted by an arrowhead (Figure 7A). In contrast to sham animals, 1-scrape and 6-scrape animal sections exhibited positivity in all regions of the disc, especially in the dorsal and ventral outer one-third AF (Figure 7B,C). Unlike 1-scrape sections, nerve fibers in 6-scrape scrape samples were commonly observed deep in the tissue along the border of the NP (Figure 7C). Advancement of nerves fibers into the interior disc structures in this model directly parallels human data in which nerves are observed to penetrate from the peripheral AF into the disc interior.[15,16] Significantly higher nerve scores were present between injured and sham animals in all regions apart from the ligamentous tissue. Summation of disc only nerve scores, that is, ventral AF, NP, and dorsal AF, affirmed an overall increase in innervation of injured discs compared to healthy discs (Figure 7E). The observations and quantifications made from nerve IHC data strongly suggest the 1-scrape and 6-scrape injury along with subsequent degeneration created a neuro-permissive environment throughout the disc, allowing aberrant nerve sprouting into all disc regions.

3.7 | Injury results in disc cell TNF- α expression

Increased inflammation is consistently observed in disc samples from patients suffering LBP suggesting it is a contributing factor to disc-associated pain.[19,68,69] To assess inflammation in this model, TNF-α was visualized in disc sections using immunohistochemistry and TNF-α + cells were counted. 1-scrape and 6-scrape disc cells exhibited immunopositivity for TNF-α especially in the ventral AF and granulation tissue (Figure 8B-IV,C-VI). Significantly increased cellular inflammation was observed in the ventral AF and ventral ligament of 6-scrape animals compared to sham (Figure 8D). The dorsal and ventral AF tissue values were then summated to get a total disc approximation of TNF-α positivity (Figure 8E). The NP was excluded from this sum due to the abnormal staining pattern which is discussed later. 6-scrape AF tissue contained significantly more TNF-α positive cells than sham discs. In conclusion, these data confirmed the injury and subsequent degeneration promoted production of TNF-α, indicative of inflammation, but further work is needed to validate these results and to determine the inflammatory state of healthy NP.

3.8 | Pain-like behavior was significantly correlated with post-processing outcomes

A Pearson correlation analysis in GraphPad Prism 9 was performed to determine how disc volume, grip strength, von Frey, pressure algometry, distance traveled, H&E, disc nerves, ligament cellularity, disc cellularity, and disc inflammation were associated with one another given the divergent progression of disc degeneration across the three treatment groups over the 18-weeks. Both of these assessments measured associations between the various outcomes and did not include treatment status. Semi-quantitative and ordinal data sets were included in this analysis because for each semi-quantitative or ordinal data point, nine measurements were averaged making all the data semi-continuous and thus useful for comparison. Twenty significant correlations were revealed among the ten selected assessment outcomes (Figure 9A). The analysis revealed that important facets of disc degeneration hypothesized to contribute to disc-associated pain in humans, like disc volume loss and nerve sprouting, were significantly correlated with pain-like behavior. The relationship between the average of the final two collections of grip strength and nerve score was highly significant ($p < 0.0004$) with a moderate correlation of -0.59 (Figure 9B). A PCA was also performed in GraphPad Prism 9 to impute factors contributing the most variability in the model's 18-week data set. Because this analysis is agnostic to treatment status, it was able to provide insight into what factors most strongly contribute to data point distribution in a blinded manner. Principal component 1 accounted for 42% of variability across all selected data sets. Assessments which were successful in detecting robust differences between injured and sham animals split along principal component 1 suggesting this component is related to injury (Figure 9C). The correlation and PCA provided crucial insight into how nerve sprouting was tied to disc-associated pain-like behavior and confirmed most

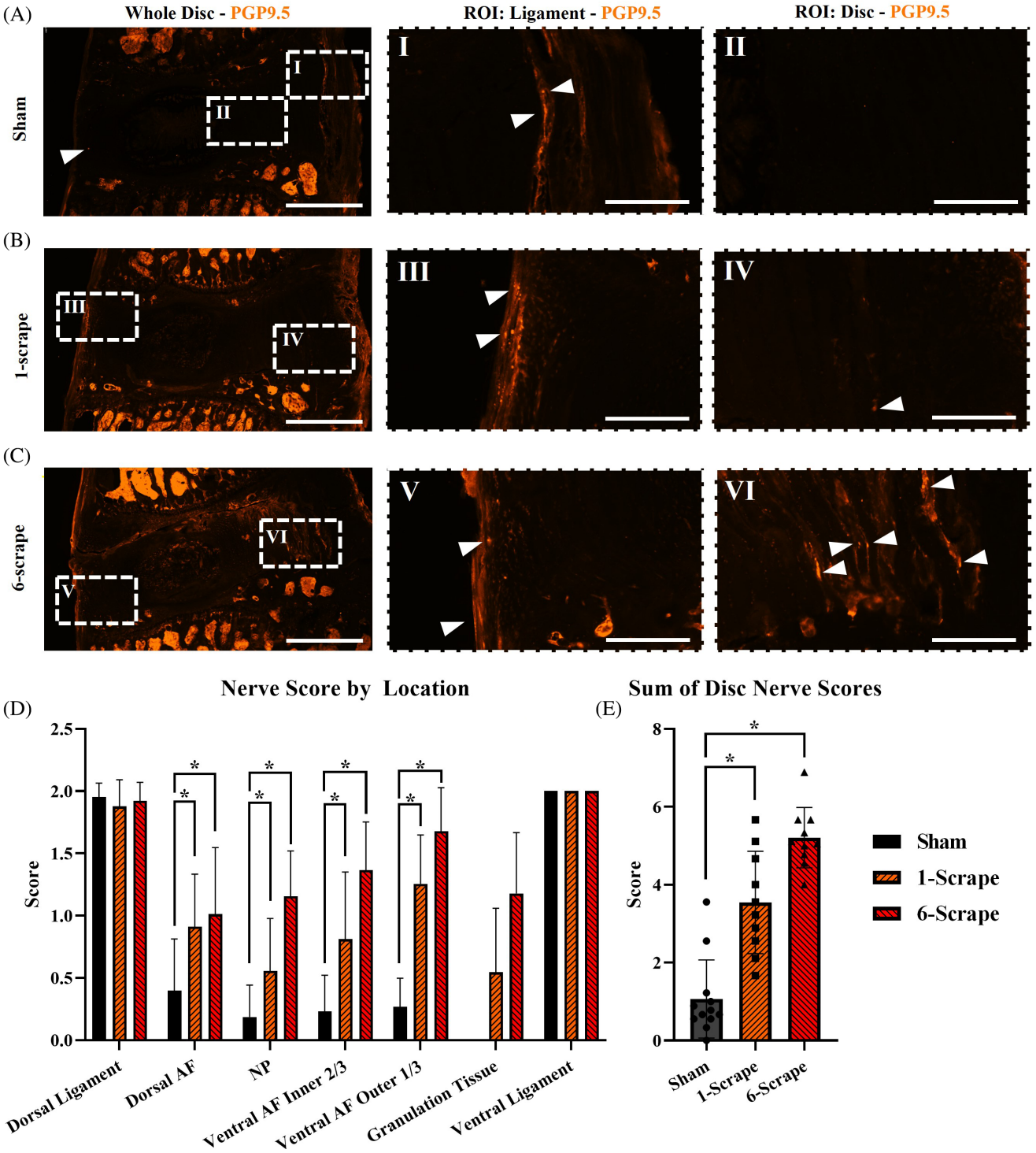

FIGURE 7 Nerves sprout into degenerated discs. Representative nerve (PGP 9.5) images from the sham group (A), 1-scrape group (B), and 6-scrape group (C). Arrowheads point to nerve fibers. PGP9.5 immunopositivity in the ligamentous tissue was used as ground truth for nerve fiber quantification. (A) Box I highlights the presence of nerve fibers located in the ventral ligament of a sham section in sham animals. Very rarely were nerve fibers observed in the discs of sham animals as shown in box II. (B) Box III shows a handful of fibers located in the dorsal ligament of 1-scrape animals. Box IV highlights the presence of a nerve fiber in the ventral AF of a 1-scrape animal. (C) Box V highlights multiple nerve fibers found in the dorsal AF of a 6-scrape section. Box VI exhibits a multitude of nerve fibers in the ventral AF of a 6-scrape animal. Whole disc image scale bar = 1 mm. ROI scale bar = 250 μm. (D) Evaluation of nerve fibers by location and treatment. 1-scrape and 6-scrape animals contained significantly more nerves than sham animals. (E) Summation of the NP and AF nerve scores. Both 1-scrape and 6-scrape nerve scores were significantly greater than sham. Data are shown as mean with standard deviation. One animal from the 1-scrape was excluded due to a lack of usable sections (n = 10–12 per group). The ventral ligamentous tissue in all animals contained 4+ nerves resulting in a standard deviation of zero. # = $p < 0.05$ sham versus 1-scrape. * = $p < 0.05$ sham versus 6-scrape

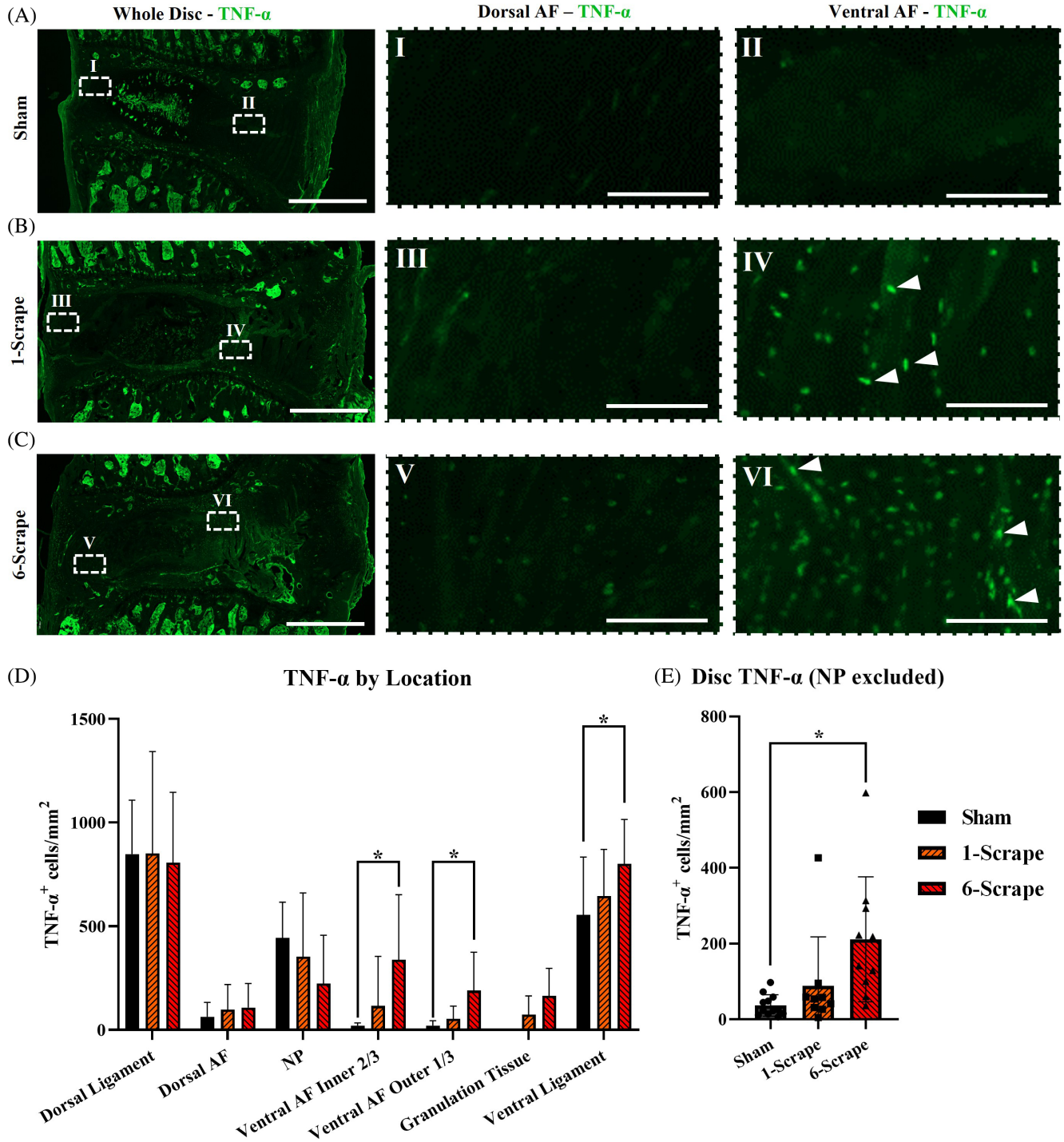

FIGURE 8 Degenerated disc cells express TNF-α. Representative TNF-α images from the sham group (A), 1-scrape group (B), and 6-scrape group (C). (A) Sham animal NPs stained extensively with TNF-α although it remains unclear if this is true immunopositivity. Sparce immunopositivity was observed in the dorsal and ventral AF of sham animals as seen in box I and II respectively. (B) 1-scrape sections contained immunopositive cells predominantly in the ventral AF, box IV, although some immunopositive cells were observed in the dorsal AF, box III. 1-scrape and 6-scrape NPs contained immunopositive areas, but this staining was fainter than sham NPs. (C) Boxes V and VI highlights immunopositivity in the dorsal and ventral AF tissue of 6-scrape animals. Arrowheads in both (B) and (C) point to cells which were strongly immunoreactive for TNF-α. Whole disc image scale bar = 1 mm. ROI scale bar = 100 μm. (D) Summary of the TNF-α cellular quantification broken down by zones. Significantly more TNF-α + cells were found in 6-scrape ventral AF and ligamentous tissue. (E) Disc total averages, excluding NP, of TNF-α + cell scores. Disc cellular TNF-α was significantly higher in 6-scrape animals compared to sham. Data are shown as mean with standard deviation. Two animals from the 1-scrape group were excluded due to a lack of usable sections ($n = 9–12$ per group). Significant differences between groups were assessed using a one-way ANOVA. # = $p < 0.05$ sham versus 1-scrape. * = $p < 0.05$ sham versus 6-scrape

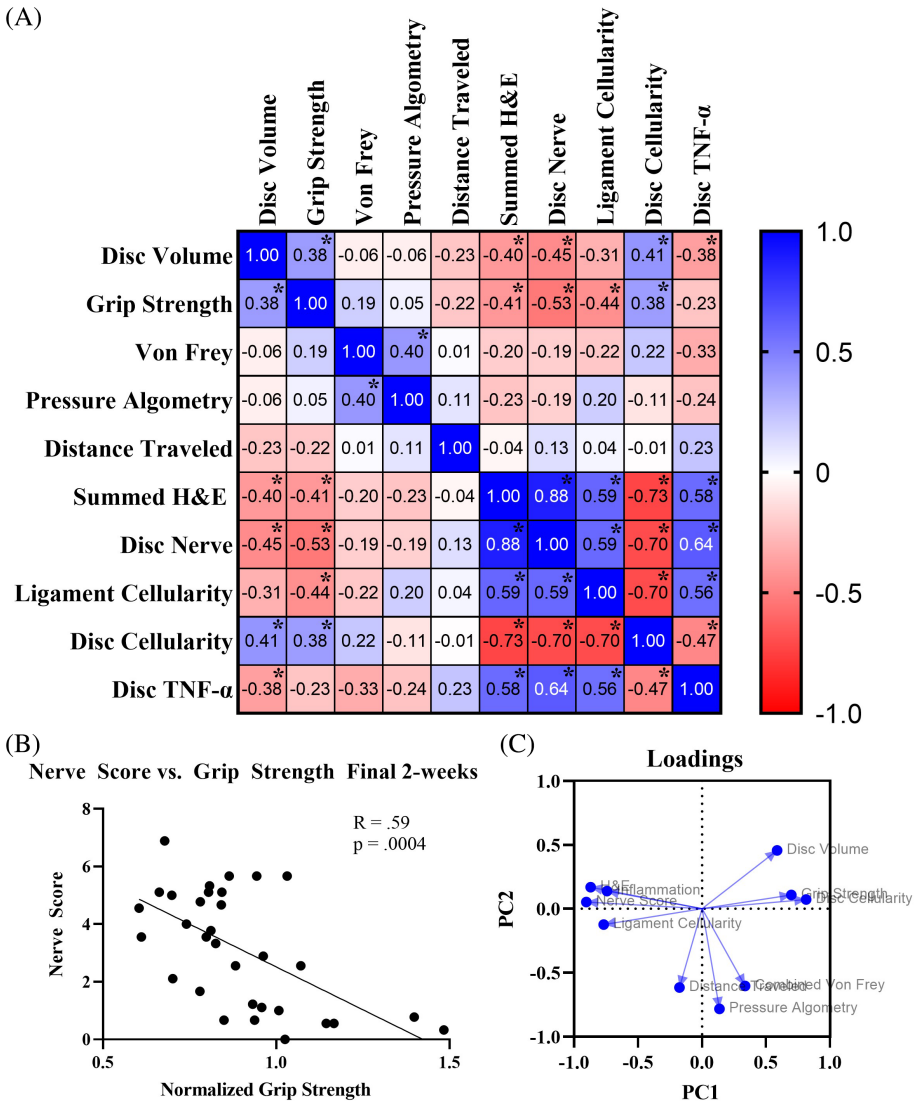

FIGURE 9 Relationships between data sets. (A) Correlation matrix of various behavioral and post-processing analyses. Strong correlations were found between grip strength and disc nerve score and among various post-processing outcomes. (B) Association between nerve score and the average grip strength in the final 2-weeks. This relationship was highly significant and moderate in strength. (C) principal component analysis loadings of the top two principal components. H&E, inflammation, nerve score, and ligament cellularity skewed negative along PC1. Disc volume, grip strength, and disc cellularity skewed positive along PC1. Pressure algometry, Von Frey, and distance traveled skewed negative along PC2. PC1 was assumed to be injury due to the distribution of assessments which were metrics of degeneration along this axis. Significant correlations between groups were assessed using a correlation analysis in Prism 9. * = $p < 0.05$

assessments were accurate in detecting differences due to injury. Furthermore, the highly significant correlation between grip strength and nerve sprouting implies that this model was successful in producing a degenerative disc pain-like phenotype.

4 | DISCUSSION

This work provides the basis of an animal model of disc-associated pain that accurately approximates the human condition. The chronic pain-like behavior, which was correlated with disc degeneration and nerve fiber sprouting, presents strong evidence that this model was successful in creating a pain-like phenotype that resulted from pathological shifts in the disc. Additionally, four important characteristics of human degenerative discs, namely, ECM breakdown, hypocellularity, inflammation, and aberrant nerve sprouting were manifested in our model, demonstrating comprehensive model validity.

Special consideration was given at the beginning of this study to develop a degeneration induction mechanism that replicates a traumatic event. The needle puncture procedure was refined using 60 rat motion segments (data not shown) to create a traumatic fissure which perforated the AF and resulted in a degenerative phenotype highly analogous to the human clinical presentation of a radiating annular tear (Figure 2C).[70] Assessing changes in the disc due to injury using μCT was important as a litmus test for injury success and to track changes in the disc real-time. At 2-weeks post-injury, the volumetric method developed in our lab (under review), detected a highly significant decrease of disc volume in injured animals compared to controls confirming successful disc injury.

Provided the knowledge that injury decreased disc volume, the next important question was if injury and ongoing degeneration resulted in pain-like behavior changes. Patients suffering LBP experience movement evoked pain, indicating mechanical agitation of the spine can exacerbate nociception.[71,72] The highly significant (week 16 and 18 $p < 0.0001$) and substantial reduction in grip strength between 6-scrape and sham animals across eight time points implied that disc injury resulted in hypersensitivity to axial strain. We believe that the grip strength assay was sensitive to degenerative changes

because the L5-L6 motion segment is the most caudal spinal structure with significant degrees of freedom involved in this assay. The L6-S1 motion segment is relatively translationally locked because it is fused to the sacrum and iliac, both of which have multiple stabilizing muscle attachments. The immobility of L6-S1 suggests that the axial stress imparted on the spine by the pulling motion disproportionately affects the L5-L6 motion segment because musculature is not present to partially distribute the load. Supporting this hypothesis, we observed a distinct increase in spinal curvature above the L5-L6 motion segment in all animals during the grip strength assay. Given the abundance of nerves in degenerated discs and these features, it is likely the axial strain led to increased nociceptor depolarizations in degenerated discs, causing cognitive or spinal reflex mechanisms to release the grip plate at a lower threshold compared to sham. Also, the persistent and progressive decrease in 6-scrape grip strength suggested underlying pathological shifts due to injury driven hypersensitivity rather than acute effects. To our knowledge, no other rat model of disc degeneration has measured increased axial hypersensitivity to this extent longitudinally. Pressure algometry was performed to provide another metric of evoked pain-like behavior. Unlike grip strength, this assay provoked the disc through shear strain rather than axial strain. Similar to a prior model of repeated disc puncture,[37] pressure algometry detected differences between sham and injured animals at multiple time points, implying that the nociceptors in the degenerative tissue were activated by shear strain albeit less so compared to axial strain. In difference to well-established models of disc degeneration,[60] we failed to detect signs of referred hypersensitivity measured by the von Frey assay. The presupposition behind this assay was that dichotomizing neurons innervating both the hind paw and the degenerated disc could be phenotypically altered by the inflammation present in the degenerated disc giving rise to hind paw referred hypersensitivity. Despite sham exhibiting higher thresholds than injured animals at all time points except week 2, these differences failed to reach significance suggesting that referred hypersensitivity was not strongly present. The discrepancy between our model and other models could be due to sex differences in pain, degree of injury, pain masking, and innervation especially considering another study witnessed similar results with von Frey characterization on female rats after disc injury.[59] Furthermore, sham animals exhibited higher withdrawal thresholds compared to injured animals at all time points, indicating that we may have lacked sufficient statistical power to detect the differences. The final method used to gauge pain-like behavior was the open field test which did not measure any significant difference.

The disc volume and behavior data suggested that injury resulted in pathological disc changes, but these pathologies were unknown. To elucidate the factors underpinning the behavioral changes, we quantified four key aspects of degeneration found in disc samples from LBP patients: ECM breakdown, hypocellularity, aberrant nerve sprouting, and inflammation. The first assessment employed was H&E analysis which is the gold standard for measuring disc degeneration and incorporates multiple metrics of ECM breakdown. End plate ossification present in all animals was consistent with previous literature which observed endplate calcification in 94% of sand rats at the equivalent spinal level and age.[73] Unexpectedly, all healthy NP lacunae stained with eosin (pink) which can be seen in Figure 4A-II, albeit slightly masked by dark hematoxylin (purple) staining. This unexpected staining indicates that NP lacunae in rats are different in charge and composition than the surrounding ECM. Additional insight was provided by H&E concerning the radial expansion and volume increase of degenerated discs noted in μCT. For healthy discs, the vertebral bodies always terminated in line with the ventral AF. However, depending on the severity of degeneration, granulation tissue up to 500 μm thick was present between the outer edge of the AF and the ventral ligament in injured discs, paralleling granulation tissue found in human degenerated discs.[74] In all cases, the granulation tissue was flanked caudal and cranial and sometimes further ventrolateral by bony deposition suggesting that it was load bearing. Gradual deposition of this granulation tissue may have been the factor that drove disc volume increase following injury.

Similar to human data, degenerated discs in our model were hypocellular with large swaths of the ventral AF in injured animals completely devoid of nuclei. Hypocellular tissue predominantly expanded around the site of needle puncture in the AF, indicating that secondary aspects of the tissue defect inhibited cellular survival. One possible explanation for this hypocellularity is that matrix catabolism resulted in deleterious loading patterns, causing apoptosis through the MAPK pathway.[75–77] Also like human degeneration, there was cellularized granulation tissue around the ventral surface of the disc.[78] We presume that the increased cellularity in the ligamentous tissue of injured animals was a result of infiltrating fibroblasts into the granulation zone.

Nerves in the disc were quantified because aberrant nerve sprouting is hypothesized as a source of painful disc degeneration. In our model, nerve sprouting was ubiquitous across degenerated discs. Because three sections were analyzed for each animal, some nerve fibers could be visualized passing between sections, confirming with high certainty the immunopositivity was indicative of nerve fibers. When present in degenerated discs, nerves were enriched around annular fissures and in areas of clear tissue disruption which directly compliments human data.[15,16,79,80] This bias in locality may be accounted for by cytokines like NGF, which is known to be produced by degenerating disc cells and stimulates neuronal ingrowth.[81] The proximity of nerves to the disrupted tissue may have predisposed them to activation during mechanical aggravation.

Inflammation proved to be most difficult to analyze in our model. Strong staining of the NP with TNF-α contradicted literature that has quantified this cytokine in degenerated and healthy discs.[68] Of note, the areas of healthy NP that were immunoreactive with the TNF-α antibody precisely aligned with the areas of healthy NP that unexpectedly stained with eosin in H&E suggesting electrostatic interactions may have driven false-positivity.[82] Abnormal IHC staining of the NP has been observed in rodents previously suggesting this staining is a false positive.[50] We also witnessed this phenomenon infrequently with other antibody targets but failed to see this phenomenon with secondary only controls (Figure S2). Despite these obstacles, we believe that counting TNF-α^{+} cells was sufficient to gather an approximation of discal inflammation.

After analysis of individual data sets, we evaluated how week 18 and post-processing data sets related to one another and how well our assessments measured differences due to injury. To answer these questions, we performed a correlation and PCA to impute relationships between data sets and contributors of variance respectively. The correlation value of 0.88 between nerve score and H&E suggested that disc breakdown was intrinsically tied to the production of a neuropermissive environment. The notion that disc volume can serve as a proxy of degeneration was validated by the significant correlation of −0.40 between H&E and disc volume. Greatly important to the validity of this work was the significant correlation of −0.59 between nerve score and grip strength. This moderate relationship provides evidence that nerve presence could be the basis for disc-associated pain. This relationship was limited by the contribution of nociceptive fibers in the granulation and ligamentous tissue, as well as changes in the facet joints, end plates, and paraspinal muscles which were not a part of the nerve score but could have contributed to overall axial hypersensitivity. The role of nerve infiltration in pain development could be further elucidated in the future by assessing this relationship longitudinally. The PCA revealed that PC1 accounted for 42% of variability across all data sets used in the correlation analysis. The Eigenvector of this component was more than double that of PC2, suggesting that it was an overwhelming contributor to assay variance. Assays which measured differences due to treatment tended to cluster on each end of the PC1 axis, indicating that this component was related to treatment.

This work has a few limitations in addition to those already mentioned. First, only female animals were employed making it unclear how sexual dimorphism may relate to the onset of disc degeneration and pain. Furthermore, animals were housed randomly implicating affect contagion as a possible confounding factor in behavioral data.[83] Finally, predictive validity was not measured to verify that the pain could be alleviated via treatments which have efficacy in humans. Work is ongoing to address these limitations in future use of this model.

In summary, construct validity was intrinsic to this model because degeneration induction mimicked an annular radiating tear, which occurs in 50% of human discs by age 35.[70] Face validity was robustly upheld by significant increases in axial hypersensitivity, deep pressure hypersensitivity, disc degeneration, inflammation, hypocellularity, and aberrant innervation. Therapies with known effects, like opioids, must be tested in the future to verify predictive validity. We hope that this model will provide utility for the advancement of translatable therapeutics and basic science around LBP which is an immense problem that plagues modern society.

AUTHOR CONTRIBUTION

David J. Lillyman – Study conceptualization, study methodology, behavioral data collection, μCT data collection, μCT data processing, tissue sectioning, IHC processing, graphic designs, statistical analysis, manuscript creation, and manuscript editing. **Fei San Lee** – Manuscript review, IHC processing, and image acquisition. **Evie C. Barnett** – Manuscript review, H&E grading, nerve IHC grading, cellularity quantification, and inflammation quantification. **Tyler J. Miller** – Manuscript review, Behavioral data collection, H&E processing, image acquisition, and μCT data collection. **Alvaro Moreno Lozano** – Manuscript review, H&E grading, and nerve IHC grading. **Henry C. Drvol** – Manuscript review, H&E grading, and nerve IHC grading. **Rebecca A. Wachs** - Study conceptualization, study methodology, behavioral data collection, manuscript review, and funding acquisition.

ACKNOWLEDGEMENTS

We acknowledge the staff at the Life Sciences Annex at the University of Nebraska – Lincoln, especially veterinarian, Anna Fitzwater, who performed the animal surgeries. This research was funded in part by the Nebraska Tobacco Settlement Biomedical Research Development Fund.

FUNDING INFORMATION

This research did not receive any specific grant from funding agencies in the public, commercial, or not-for-profit sectors.

CONFLICT OF INTEREST

The authors declare no conflicts of interest.

ORCID

David J. Lillyman https://orcid.org/0000-0002-2470-5473

REFERENCES

1. James SL, Abate D, Abate KH, et al. Global, regional, and national incidence, prevalence, and years lived with disability for 354 diseases and injuries for 195 countries and territories, 1990–2017: a systematic analysis for the global burden of disease study 2017. *The Lancet*. 2018;*392*(10159):1789-1858.
2. Hestbaek L, Leboeuf-Yde C, Manniche C. Low back pain: what is the long-term course? A review of studies of general patient populations. *Eur Spine J*. 2003;*12*(2):149-165. doi:10.1007/s00586-002-0508-5
3. Martin BI, Deyo RA, Mirza SK, et al. Expenditures and health status among adults with back and neck problems. *Jama*. 2008;*299*(6):656-664.
4. Racine M. Chronic pain and suicide risk: a comprehensive review. *Progress Neuro-Psychopharmacol Biol Psych*. 2018;*87*:269–280. doi:10.1016/j.pnpbp.2017.08.020 Accessed December 20, 2018.
5. Shmagel A, Foley R, Ibrahim H. Epidemiology of chronic Low Back pain in US adults: data from the 2009-2010 National Health and nutrition examination survey. *Arthritis Care Res (Hoboken)*. 2016;*68*(11):1688-1694. doi:10.1002/acr.22890
6. DePalma MJ, Ketchum JM, Saullo T. What is the source of chronic low back pain and does age play a role? *Pain Med*. 2011;*12*(2):224-233.
7. Maher CG. Effective physical treatment for chronic low back pain. *Orthop Clin North Am*. 2004;*35*(1):57-64. doi:10.1016/s0030-5898(03)00088-9
8. Fritzell P, Hägg O, Wessberg P, Nordwall A, Group SLSS. Chronic low back pain and fusion: a comparison of three surgical techniques: a prospective multicenter randomized study from the Swedish lumbar spine study group. *Spine*. 2002;*27*(11):1131-1141.
9. Lu Y, Guzman JZ, Purmessur D, et al. Nonoperative management of discogenic back pain: a systematic review. *Spine*. 2014;*39*(16):1314-1324. doi:10.1097/BRS.0000000000000401
10. Martin MD, Boxell CM, Malone DG. Pathophysiology of lumbar disc degeneration: a review of the literature. *Neurosurg Focus*. 2002;*13*(2):1-6.

11. Mohanty S, Dahia CL. Defects in intervertebral disc and spine during development, degeneration, and pain: new research directions for disc regeneration and therapy. *Wiley Interdiscip Rev Dev Biol*. 2019; *8*(4):e343. doi:10.1002/wdev.343
12. Altun I. Cytokine profile in degenerated painful intervertebral disc: variability with respect to duration of symptoms and type of disease. *Spine J* 2016;*16*(7):857–861. 10.1016/j.spinee.2016.03.019 Accessed July 1, 2016.
13. Peng B-G. Pathophysiology, diagnosis, and treatment of discogenic low back pain. *World J Orthop*. 2013;*4*(2):42-52. doi:10.5312/wjo.v4.i2.42
14. Vo NV, Hartman RA, Yurube T, Jacobs LJ, Sowa GA, Kang JD. Expression and regulation of metalloproteinases and their inhibitors in intervertebral disc aging and degeneration. *Spine J*. 2013;*13*(3):331-341. doi:10.1016/j.spinee.2012.02.027
15. Binch ALA, Cole AA, Breakwell LM, et al. Nerves are more abundant than blood vessels in the degenerate human intervertebral disc. *Arthritis Res Ther*. 2015;*17*(1):370. doi:10.1186/s13075-015-0889-6 Accessed December 21, 2015.
16. Coppes MH, Marani E, Thomeer RT, Groen GJ. Innervation of "painful" lumbar discs. *Spine (Phila pa 1976)*. 1997;*22*(20):2342-2349. doi:10.1097/00007632-199710150-00005
17. García-Cosamalón J, del Valle ME, Calavia MG, et al. Intervertebral disc, sensory nerves and neurotrophins: who is who in discogenic pain? *J Anat*. 2010;*217*(1):1-15. doi:10.1111/j.1469-7580.2010.01227.x
18. De Geer CM. Intervertebral disk nutrients and transport mechanisms in relation to disk degeneration: a narrative literature review. *J Chiropr Med*. 2018;*17*(2):97-105. doi:10.1016/j.jcm.2017.11.006
19. Burke JG, Watson RW, McCormack D, Dowling FE, Walsh MG, Fitzpatrick JM. Intervertebral discs which cause low back pain secrete high levels of proinflammatory mediators. *J Bone Joint Surg*. 2002; *84*(2):196-201. doi:10.1302/0301-620x.84b2.12511
20. Berge O-G. Predictive validity of behavioural animal models for chronic pain. *Br J Pharmacol*. 2011;*164*(4):1195–1206. doi:10.1111/j.1476-5381.2011.01300.x Accessed October 1, 2011
21. Denayer T, Stöhr T, Van Roy M. Animal models in translational medicine: validation and prediction. *New Horiz Transl Med*. 2014;*2*(1):5-11.
22. Blackburn-Munro G. Pain-like behaviours in animals–how human are they? *Trends Pharmacol Sci*. 2004;*25*(6):299-305.
23. Deuis JR, Dvorakova LS, Vetter I. Methods used to evaluate pain behaviors in rodents. *Front Mol Neurosci*. 2017;*10*:284. doi:10.3389/fnmol.2017.00284
24. Kettler A, Liakos L, Haegele B, Wilke HJ. Are the spines of calf, pig and sheep suitable models for pre-clinical implant tests? *Eur Spine J* 2007;*16*(12):2186–2192. doi:10.1007/s00586-007-0485-9 Accessed December 1, 2007
25. Wilke HJ, Neef P, Caimi M, Hoogland T, Claes LE. New in vivo measurements of pressures in the intervertebral disc in daily life. *Spine (Phila pa 1976)*. 1999;*24*(8):755-762. doi:10.1097/00007632-199904150-00005
26. Guehring T, Unglaub F, Lorenz H, Omlor G, Wilke H-J, Kroeber MW. Intradiscal pressure measurements in normal discs, compressed discs and compressed discs treated with axial posterior disc distraction: an experimental study on the rabbit lumbar spine model. *Eur Spine J*. 2006;*15*(5):597-604. doi:10.1007/s00586-005-0953-z
27. Riches PE, Dhillon N, Lotz J, Woods AW, McNally DS. The internal mechanics of the intervertebral disc under cyclic loading. *J Biomech*. 2002;*35*(9):1263-1271. doi:10.1016/s0021-9290(02)00070-2
28. Kuo YW, Wang JL. Rheology of intervertebral disc: an ex vivo study on the effect of loading history, loading magnitude, fatigue loading, and disc degeneration. *Spine (Phila pa 1976)*. 2010;*35*(16):E743-E752. doi:10.1097/BRS.0b013e3181d7a839
29. Nikkhoo M, Kargar R, Khalaf K. *Biphasic rheology of different artificial degenerated intervertebral discs*. Springer; 2019:671-674.
30. Beckstein JC, Sen S, Schaer TP, Vresilovic EJ, Elliott DM. Comparison of animal discs used in disc research to human lumbar disc: axial compression mechanics and glycosaminoglycan content. *Spine (Phila pa 1976)*. 2008;*33*(6):E166-E173. doi:10.1097/BRS.0b013e318166e001
31. Lin KH, Wu Q, Leib DJ, Tang SY. A novel technique for the contrast-enhanced microCT imaging of murine intervertebral discs. *J Mech Behav Biomed Mater* 2016;*63*:66–74. doi:10.1016/j.jmbbm.2016.06.003 Accessed October 1, 2016.
32. Lee M, Kim B-J, Lim EJ, et al. Complete Freund's adjuvant-induced intervertebral discitis as an animal model for Discogenic Low Back pain. *Anesthesia & Analgesia*. 2009;*109*(4):1287-1296.
33. Glaeser JD, Tawackoli W, Ju DG, et al. Optimization of a rat lumbar IVD degeneration model for low back pain. *Jor Spine*. 2020;*3*(2): e1092. doi:10.1002/jsp2.1092 Accessed June 1, 2020.
34. Liu Q, Wang X, Hua Y, et al. Estrogen deficiency exacerbates intervertebral disc degeneration induced by spinal instability in rats. *Spine*. 2019;*44*(9):E510-E519.
35. Leimer EM, Gayoso MG, Jing L, Tang SY, Gupta MC, Setton LA. Behavioral compensations and neuronal remodeling in a rodent model of chronic intervertebral disc degeneration. *Sci Rep* 2019;*9*(1):3759. doi:10.1038/s41598-019-39657-6 Accessed March 6, 2019.
36. Li Z, Liu H, Yang H, et al. Both expression of cytokines and posterior annulus fibrosus rupture are essential for pain behavior changes induced by degenerative intervertebral disc: an experimental study in rats. *J Orthop Res*. 2014;*32*(2):262-272.
37. Muralidharan A, Park TS, Mackie JT, et al. Establishment and characterization of a novel rat model of mechanical low back pain using behavioral, pharmacologic and histologic methods. *Front Pharmacol*. 2017;*8*:493.
38. Lai A, Ho L, Evashwick-Rogler TW, et al. Dietary polyphenols as a safe and novel intervention for modulating pain associated with intervertebral disc degeneration in an in-vivo rat model. *PLOS One*. 2019; *14*(10):e0223435. doi:10.1371/journal.pone.0223435
39. Lai A, Gansau J, Gullbrand SE, et al. Development of a standardized histopathology scoring system for intervertebral disc degeneration in rat models: an initiative of the ORS spine section. *JOR Spine*. 2021;*4*: e1150.
40. Levenfus I. *An efficient method for counting DAPI-stained cells using Fiji*. GRIN Verlag; 2011.
41. Mosley GE, Evashwick-Rogler TW, Lai A, Iatridis JC. Looking beyond the intervertebral disc: the need for behavioral assays in models of discogenic pain. *Ann N Y Acad Sci*. 2017;*1409*(1):51-66. doi:10.1111/nyas.13429
42. Jin L, Balian G, Li XJ. Animal models for disc degeneration-an update. *Histol Histopathol*. 2018;*33*(6):543-554. doi:10.14670/HH-11-910
43. Wáng YXJ, Wáng J-Q, Káplár Z. Increased low back pain prevalence in females than in males after menopause age: evidences based on synthetic literature review. *Quant Imaging Med Surg*. 2016;*6*(2):199-206. doi:10.21037/qims.2016.04.06
44. DeMoss DL, Wright GL. Sex and strain differences in whole skeletal development in the rat. *Calcif Tissue Int*. 1998;*62*(2):153-157. doi:10.1007/s002239900409
45. Teraguchi M, Yoshimura N, Hashizume H, et al. Prevalence and distribution of intervertebral disc degeneration over the entire spine in a population-based cohort: the Wakayama spine study. *Osteoarthr Cartil* 2014;*22*(1):104–110. doi:10.1016/j.joca.2013.10.019 Accessed January 1, 2014.
46. Adams MA, Dolan P. Intervertebral disc degeneration: evidence for two distinct phenotypes. *J Anatomy*. 2012;*221*(6):497–506. doi:10.1111/j.1469-7580.2012.01551.x Accessed December 1, 2012.
47. Takeshita H, Yamamoto K, Nozato S, et al. Modified forelimb grip strength test detects aging-associated physiological decline in skeletal muscle function in male mice. *Sci Rep*. 2017;7:42323. doi:10.1038/srep42323

48. Urits I, Burshtein A, Sharma M, et al. Low back pain, a comprehensive review: pathophysiology, diagnosis, and treatment. *Curr Pain Headache Rep*. 2019;*23*(3):1-10.
49. Lee SC. Percutaneous intradiscal treatments for discogenic pain. *Acta Anaesthesiol Taiwan*. 2012;*50*(1):25-28.
50. Millecamps M, Stone LS. Delayed onset of persistent discogenic axial and radiating pain after a single-level lumbar intervertebral disc injury in mice. *Pain*. 2018;*159*(9):1843-1855.
51. Millecamps M, Tajerian M, Naso L, Sage EH, Stone LS. Lumbar intervertebral disc degeneration associated with axial and radiating low back pain in ageing SPARC-null mice. *Pain*. 2012;*153*(6):1167-1179.
52. Vatine J-J, Shapira SC, Magora F, Adler D, Magora A. Electronic pressure algometry of deep pain in healthy volunteers. *Arch Phys Med Rehabil*. 1993;*74*(5):526-530. doi:10.1016/0003-9993(93)90118-T
53. Neziri AY, Curatolo M, Limacher A, et al. Ranking of parameters of pain hypersensitivity according to their discriminative ability in chronic low back pain. *Pain* 2012;*153*(10):2083–2091. doi:10.1016/j.pain.2012.06.025 Accessed October 1, 2012
54. Takahashi Y, Chiba T, Kurokawa M, Aoki Y. Dermatomes and the central organization of dermatomes and body surface regions in the spinal cord dorsal horn in rats. *J Comp Neurol*. 2003;*462*(1):29-41. doi:10.1002/cne.10669
55. Aoki Y, Takahashi Y, Takahashi K, et al. Sensory innervation of the lateral portion of the lumbar intervertebral disc in rats. *Spine J*. 2004;*4*(3):275-280.
56. Ohtori S, Takahashi Y, Takahashi K, et al. Sensory innervation of the dorsal portion of the lumbar intervertebral disc in rats. *Spine (Phila pa 1976)*. 1999;*24*(22):2295-2299. doi:10.1097/00007632-199911150-00002
57. Malykhina AP, Qin C, Greenwood-van Meerveld B, Foreman RD, Lupu F, Akbarali HI. Hyperexcitability of convergent colon and bladder dorsal root ganglion neurons after colonic inflammation: mechanism for pelvic organ cross-talk. *Neurogastroenterol Motil*. 2006;*18*(10):936–948. doi:10.1111/j.1365-2982.2006.00807.x Accessed October 1, 2006.
58. Ustinova EE, Fraser MO, Pezzone MA. Colonic irritation in the rat sensitizes urinary bladder afferents to mechanical and chemical stimuli: an afferent origin of pelvic organ cross-sensitization. *Am J Physiol Renal Physiol*. 2006;*290*(6):F1478-F1487.
59. Mosley GE, Wang M, Nasser P, et al. Males and females exhibit distinct relationships between intervertebral disc degeneration and pain in a rat model. *Sci Rep* 2020;*10*(1):15120. doi:10.1038/s41598-020-72081-9 Accessed September 15, 2020.
60. Lai A, Moon A, Purmessur D, et al. Annular puncture with tumor necrosis factor-alpha injection enhances painful behavior with disc degeneration in vivo. *Spine J*. 2016;*16*(3):420-431.
61. Hyodo H, Sato T, Sasaki H, Tanaka Y. Discogenic pain in acute nonspecific low-back pain. *Eur Spine J*. 2005;*14*(6):573-577.
62. Jay Lipson S, Muir H. Experimental intervertebral disc degeneration. Morphologic and proteoglycan changes over time. *Arthrit Rheumat Off J Am Coll Rheumatol*. 1981;*24*(1):12-21.
63. Goldstein ME, House SB, Gainer H. NF-L and peripherin immunoreactivities define distinct classes of rat sensory ganglion cells. *J Neurosci Res*. 1991;*30*(1):92-104. doi:10.1002/jnr.490300111
64. Fornaro M, Lee JM, Raimondo S, Nicolino S, Geuna S, Giacobini-Robecchi M. Neuronal intermediate filament expression in rat dorsal root ganglia sensory neurons: an in vivo and in vitro study. *Neuroscience* 2008; *153*(4):1153–1163. doi:10.1016/j.neuroscience.2008.02.080 Accessed June 2, 2008.
65. Hammond DL, Ackerman L, Holdsworth R, Elzey B. Effects of spinal nerve ligation on immunohistochemically identified neurons in the L4 and L5 dorsal root ganglia of the rat. *J Compar Neurol*. 2004;*475*(4):575–589. doi:10.1002/cne.20209 Accessed August 2, 2004.
66. Price TJ, Louria MD, Candelario-Soto D, et al. Treatment of trigeminal ganglion neurons in vitro with NGF, GDNF or BDNF: effects on neuronal survival, neurochemical properties and TRPV1-mediated neuropeptide secretion. *BMC Neurosci*. 2005;*6*(1):1-15.
67. Pionchon H, Tommasi M, Pialat J, et al. Study of the innervation of the spinal ligaments at the lumbar level. *Bulletin de l'Association Des Anatomistes*. 1986;*70*(210):63-7. Etude de l'innervation des ligaments rachidiens à l'étage lombaire
68. Weiler C, Nerlich AG, Bachmeier BE, Boos N. Expression and distribution of tumor necrosis factor alpha in human lumbar intervertebral discs: a study in surgical specimen and autopsy controls. *Spine*. 2005;*30*(1):44-53.
69. Lyu F-J, Cui H, Pan H, et al. Painful intervertebral disc degeneration and inflammation: from laboratory evidence to clinical interventions. *Bone Res* 2021;*9*(1):7. doi:10.1038/s41413-020-00125-x Accessed January 29, 2021.
70. Osti OL, Vernon-Roberts B, Moore R, Fraser RD. Annular tears and disc degeneration in the lumbar spine. A post-mortem study of 135 discs. *J Bone Joint Surg*. 1992;*74-B*(5):678–682. doi:10.1302/0301-620X.74B5.1388173 Accessed September 1, 1992.
71. Wang W-e, Ho RLM, Gatto B, et al. Cortical dynamics of movement-evoked pain in chronic low back pain. *J Physiol*. 2021;*599*(1):289–305. doi:10.1113/JP280735 Accessed January 1, 2021.
72. Young S, Aprill C, Laslett M. Correlation of clinical examination characteristics with three sources of chronic low back pain. *Spine J* 2003;*3*(6):460–465. doi:10.1016/S1529-9430(03)00151-7 Accessed November 1, 2003.
73. Gruber HE, Gordon B, Williams C, Norton HJ, Hanley EN Jr. Vertebral endplate and disc changes in the aging sand rat lumbar spine: cross-sectional analyses of a large male and female population. *Spine (Phila pa 1976)*. 2007;*32*(23):2529-2536. doi:10.1097/BRS.0b013e318158cd69
74. Peng B, Hao J, Hou S, et al. Possible pathogenesis of painful intervertebral disc degeneration. *Spine*. 2006;*31*(5):560-566.
75. Xu Q, Fang H, Zhao L, Zhang C, Zhang L, Tian B. Mechano growth factor attenuates mechanical overload-induced nucleus pulposus cell apoptosis through inhibiting the p38 MAPK pathway. *Biosci Rep*. 2019;*39*(3):BSR20182462.
76. He R, Wang Z, Cui M, et al. HIF1A alleviates compression-induced apoptosis of nucleus pulposus derived stem cells via upregulating autophagy. *Autophagy*. 2021;*17*(11):3338-3360. doi:10.1080/15548627.2021.1872227
77. Zhuo Y, Wang H, Zou L, et al. SIRT1 attenuates apoptosis of nucleus pulposus cells by targeting interactions between LC3B and Fas under high-magnitude compression. *Oxid Med Cell Longev*. 2021;*2021*:2420969. doi:10.1155/2021/2420969
78. Torre OM, Mroz V, Bartelstein MK, Huang AH, Iatridis JC. Annulus fibrosus cell phenotypes in homeostasis and injury: implications for regenerative strategies. *Ann N Y Acad Sci*. 2019;*1442*(1):61-78.
79. Freemont AJ, Peacock TE, Goupille P, Hoyland JA, O'Brien J, Jayson MIV. Nerve ingrowth into diseased intervertebral disc in chronic back pain. *Lancet* 1997;*350*(9072):178–181. doi:10.1016/S0140-6736(97)02135-1 Accessed July 19, 1997.
80. Lama P, Le Maitre CL, Harding IJ, Dolan P, Adams MA. Nerves and blood vessels in degenerated intervertebral discs are confined to physically disrupted tissue. *J Anat*. 2018;*233*(1):86-97.
81. Richardson SM, Purmessur D, Baird P, Probyn B, Freemont AJ, Hoyland JA. Degenerate human nucleus pulposus cells promote neurite outgrowth in neural cells. *PloS ONE*. 2012;*7*(10):e47735. doi:10.1371/journal.pone.0047735
82. Wang M, Zhu D, Zhu J, Nussinov R, Ma B. Local and global anatomy of antibody-protein antigen recognition. *J Mol Recognit*. 2018;*31*(5):e2693. doi:10.1002/jmr.2693

83. Hernandez-Lallement J, Gómez-Sotres P, Carrillo M. Towards a unified theory of emotional contagion in rodents—A meta-analysis. *Neurosci Biobehav Rev* 2020;doi:10.1016/j.neubiorev.2020.09.010, *132*, 1229, 1248 Accessed October 3, 2020.

SUPPORTING INFORMATION

Additional supporting information can be found online in the Supporting Information section at the end of this article.

How to cite this article: Lillyman, D. J., Lee, F. S., Barnett, E. C., Miller, T. J., Alvaro, M. L., Drvol, H. C., & Wachs, R. A. (2022). Axial hypersensitivity is associated with aberrant nerve sprouting in a novel model of disc degeneration in female Sprague Dawley rats. *JOR Spine*, *5*(3), e1212. https://doi.org/10.1002/jsp2.1212